Femtosecond Collisional Dissipation of Vibrating D_2^+ in Helium Nanodroplets

Junjie Qiang,[1,2] Lianrong Zhou,[1] Yigeng Peng,[3] Chao Yu,[3] Peifen Lu,[1] Shengzhe Pan,[1] Chenxu Lu,[1] Gang Chen,[2] Ruifeng Lu,[3] Wenbin Zhang,[1,*] and Jian Wu[1,4,5,6,†]

[1]*State Key Laboratory of Precision Spectroscopy, East China Normal University, Shanghai 200241, China*
[2]*School of Physics and Microelectronics Key Laboratory of Materials Physics of Ministry of Education, Zhengzhou University, Zhengzhou 450001, China*
[3]*Department of Applied Physics, Nanjing University of Science and Technology, Nanjing 210094, China*
[4]*Collaborative Innovation Center of Extreme Optics, Shanxi University, Taiyuan, Shanxi 030006, China*
[5]*Chongqing Key Laboratory of Precision Optics, Chongqing Institute of East China Normal University, Chongqing 401121, China*
[6]*CAS Center for Excellence in Ultra-Intense Laser Science, Shanghai 201800, China*

(Received 16 May 2023; accepted 5 February 2024; published 4 March 2024)

We explored the collision-induced vibrational decoherence of singly ionized D_2 molecules inside a helium nanodroplet. By using the pump-probe reaction microscopy with few-cycle laser pulses, we captured in real time the collision-induced ultrafast dissipation of vibrational nuclear wave packet dynamics of D_2^+ ion embedded in the droplet. Because of the strong coupling of excited molecular cations with the surrounding solvent, the vibrational coherence of D_2^+ in the droplet interior only lasts for a few vibrational periods and completely collapses within 140 fs. The observed ultrafast coherence loss is distinct from that of isolated D_2^+ in the gas phase, where the vibrational coherence persists for a long time with periodic quantum revivals. Our findings underscore the crucial role of ultrafast collisional dissipation in shaping the molecular decoherence and solvation dynamics during solution chemical reactions, particularly when the solute molecules are predominantly in ionic states.

DOI: 10.1103/PhysRevLett.132.103201

As an important driving force for chemical reactions in dense gases or liquids, the collisional interaction can induce energy transfer among the reacting entities through quantum coherences and decoherences [1,2], which plays a key role in many-body physics [3] and solution chemistry [4–6]. For a molecule embedded in a dissipative environment, the collisions with its surroundings may largely dissipate the coherence of nuclear motions. This would degrade the phase coherences of molecular entities, leading to an irreversible influence on the chemical reactions. In general, the collisional effect on the interacting molecules strongly depends on the immediate environment. In rarefied gas, the negligible intermolecular collisions of near-isolated molecules permit a long-lived coherence of the molecular quantum dynamics [7,8]. However, in dense gases, the significant collisional dissipation will induce a fast decay of the coherent nuclear motions. For instance, the collision-induced coherence loss of molecular echo response in high-pressure dense gases suggests a timescale of the collisional dissipation dynamics on the order of a few picoseconds [9–11]. For molecules dissolved in a liquid, a more severe collisional effect is expected due to the much higher randomness and matrix density of the surrounding solvent [12–14].

The quantum liquid of superfluid helium nanodroplets (He_N) gives an expectation that the environmental collision has an inappreciable perturbation on the nuclear dynamics [15–19]. Using the solvent of He_N as an ideal reaction matrix, many studies on how the dissipative solution environment influences the nuclear motions, such as vibration [20], rotation [21,22], as well as dissociative reaction dynamics [23,24], have been conducted. For instance, the long-lived nuclear coherences of vibrational dynamics have been observed for alkali-metal dimers on droplet surfaces (range from ~5 ps to ~1.5 ns) [18,19], and for neutral indium dimers embedded in the droplet interior (tens of ps) [17]. These observations highlight the low perturbing character of He_N when comparing the observed long-lasting vibrational coherences to that in other condensed mediums, such as high-pressure buffer gases [11] and cryogenic rare-gas matrices [25], where the vibrational coherence loss typically proceeds within hundreds of femtoseconds up to a few picoseconds [26].

In principle, the collisional effect on the nuclear coherence of solute molecules in a liquid environment is largely determined by the coupling of dopants with the solvent. The collisional interaction degree depends on many aspects of the molecule's intrinsic characteristics, such as vibrational energies and modes, translational energies, electronic structures, interaction potentials, and charge states [27,28]. A strong suppression of vibrational coherence has been observed for excited lithium iodide molecules solvated in the He_N interior [20], stressing the role of molecular

excitation in the collisional dissipation. As compared to neutrals, when the charged species is embedded in He_N, due to its ionic character and excited vibrational modes, a more intensive coupling with the surroundings is expected [29,30]. However, previous investigations on the behaviors of embedding excited molecular ions are limited in spectroscopy studies [29,30]. So far, the details of how the intensive coupling between the charged ions with the helium surroundings dissipates the nuclear motions have escaped real-time observation at the molecular level. To resolve the ultrafast collisional dissipation dynamics in time domain, an observable coherence loss of nuclear motions with a shorter coherent period than the collisional decoherence time is required.

In this Letter, we used the intrinsic vibrational motion of singly ionized D_2 molecules, with a vibrational period of ~27 fs, as a sensitive probe to study the ultrafast collisional dissipation dynamics of charged molecular cation inside a He_N. By performing pump-probe experiments with few-cycle laser pulses in a reaction microscope, we compared the vibrational dynamics of D_2^+ ion in the gas-phase and in the droplet interior. The forth-and-back vibrational motion of D_2^+ induced by a pump pulse is visualized in real time by monitoring its subsequent dissociation induced by a probe pulse. Our results show that the vibrational oscillations of in-droplet D_2^+ only persist for a few periods and then quickly undergo irreversible coherence loss within ~140 fs, which is distinct from the observed long-lived vibrational coherence in gas phase. It indicates a strong coupling of the molecular cation with the liquid helium surroundings. A simplified theoretical model was developed to understand the D_2^+-He collisional interaction.

As depicted in Fig. 1(a), the experimental measurements were performed in a reaction microscope of cold target recoil ion momentum spectroscopy (COLTRIMS) [31]. The helium nanodroplets, containing on average ~1800 He atoms [32], were doped with one D_2 molecule (see more details in the Supplemental Material [33]). As illustrated in Fig. 1(b), a linearly polarized femtosecond laser pulse (790 nm, 25 fs, 10 kHz) was spectrally broadened via a multiple-plate continuum generation system [44], and afterwards temporally compressed to produce 8-fs few-cycle pulses for the pump-probe experiments. The pump-probe scheme for probing the collisional dissipation dynamics is illustrated in Fig. 1(c), which is based on the laser-induced dissociative ionization of D_2 molecules. First, the ultrashort pump pulse removes one electron from a neutral D_2 molecule, launching a vibrational nuclear wave packet (NWP) moving initially on the ground $1s\sigma_g$ state of D_2^+. The propagating NWP that may undergo a photon-coupled transition to the upper $2p\sigma_u$ state at the internuclear distance of R_c, which is subsequently fragmentized by a probe pulse through either dissociating into D^+ and D [45], denoted as $D_2(1,0)$ channel, or Coulomb exploding into D^+ and D^+ [46]. The vibrational motion of

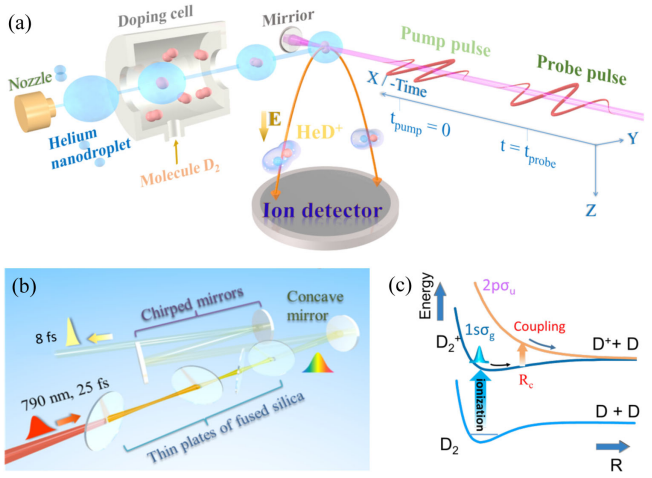

FIG. 1. (a) Schematic diagram of the experimental setup for femtosecond pump-probe reaction microscopy. (b) Sketch of the few-cycle laser pulse generation system. The four thin fused silica plates, placed near the waist of the beam at Brewster's angle, were used to generate an ultrafast white light continuum. The dispersion introduced by silica plates was compensated by the chirped mirror pairs. (c) Potential energy curves of D_2 and D_2^+, illustrating the process of pump-probe-induced dissociative ionization of D_2 molecules.

D_2^+ NWP can be visualized by measuring the time-dependent D^+ ion yields resulting from the two fragmentation channels [40,47]. The observed time-resolved vibrational coherence loss allows manifesting the collisional effect in the dissipative environment.

In the experiment, due to the diffusion of free molecules from the pickup cell to the target region, the molecular beam in the interaction region contains D_2 molecules in gas phase and embedded in the He_N interior. Both the gas-phase and in-droplet D_2 molecules will interact with the laser pulses to generate D^+ fragment ions. To identify the right He_N events, we recorded the He_nD^+ $(n = 1, 2, 3, \ldots)$ ions rather than pure D^+ ions to account for the dissociative ionization of in-droplet D_2 molecules [15]. Figure 2(a) shows the measured yields of ion fragments as a function of their time-of-flight (TOF) and impact positions along the y axis of the detector, integrated over the pump-probe time delay. In the spectrum, the D^+ $(m/q = 2)$ ions, mainly resulting from the $D_2(1,0)$ channel of gas-phase D_2, and the HeD^+ $(m/q = 6)$, He_2D^+ $(m/q = 10)$ ions, originating from the dissociative ionization of in-droplet D_2, can be clearly distinguished, and were selected for further analysis.

Figures 2(b)–2(e) display the laser-shot-normalized yields of D^+, HeD^+, and He_2D^+ ions as a function of the pump-probe time delay within different time windows. We first inspected the time-dependent yield distributions of D^+ from the breaking of gas-phase D_2^+ ions. Three major features are exhibited. First, as indicated by the three black arrows in Fig. 2(b), well-resolved oscillatory structures peaking at ~38, 66, and 93 fs, with a period of $T \sim 27$ fs,

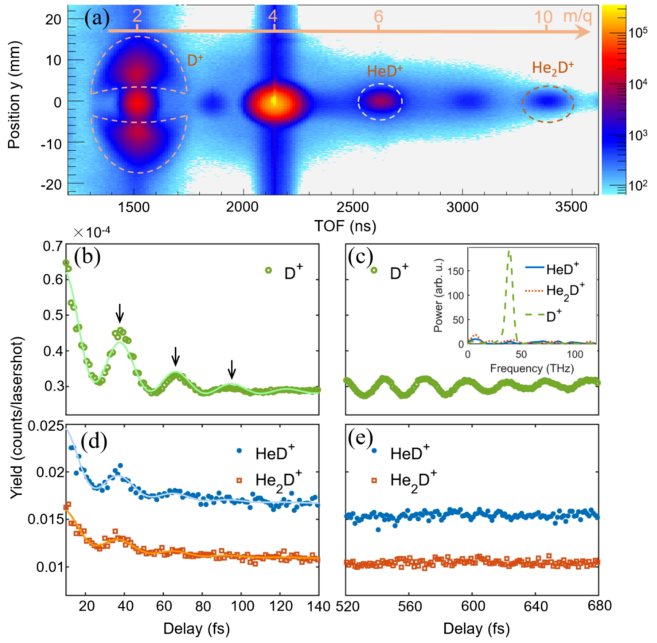

FIG. 2. (a) Time-integrated ion yields as a function of their TOF and positions measured in the pump-probe experiments. The signal islands, indicated by dashed ellipses, with $m/q = 2$ (1300 ns < TOF < 1750 ns), $m/q = 6$ (2500 ns < TOF < 2800 ns), and $m/q = 10$ (3250 ns < TOF < 3550 ns), are assigned to D^+, HeD^+, and He_2D^+ ions, respectively. (b),(d) Measured yields of different fragment ions: D^+, HeD^+, He_2D^+, as a function of the pump-probe time delay. The solid lines are numerical fits to the data points. (c),(e) Time-dependent ion yields of D^+, HeD^+, and He_2D^+ for time window from 520 to 680 fs. The corresponding FFT spectra are shown in the inset. Each data point of the ion yield distributions from (b) to (e) is normalized to a single laser shot.

can be observed. Second, the vibrational structures in Fig. 2(b) exhibit apparent damped oscillations with decreasing contrast. Third, as shown in Fig. 2(c), an obvious vibrational structure reappears between 520 and 680 fs for the D^+ yield distribution. These features manifest the vibrational motion of the bound D_2^+ NWP. Initially, the D_2^+ NWPs are populated onto various vibrational states. The dominating coherences between neighboring vibrational states with different frequencies lead to the oscillatory peak structures in the time domain. The vibrational NWP then undergoes dispersion during its oscillatory motion between the outer and inner turning points. Because of the anharmonicity of the potential curve of the D_2^+ ground state [40], the vibrational contributions at different frequencies gradually get out of phase, leading to the apparent degeneration of the vibrational structures. However, since the vibrational motion of the isolated gas phase D_2^+ is nondisturbed by the environment, the vibrational NWP stays fully coherent despite its dispersion. The restored periodicity of the vibrational motion at large delay [Fig. 2(c)] thus reflects the quantum vibrational revival of the D_2^+ NWP [48,49]. Note that the low revival amplitude can be attributed to the excitation of rotational NWP of gas-phase D_2^+ [33,40].

Using the observed vibrational motion of the gas-phase D_2^+ as a reference, we now turn our attention to the vibrational dynamics of D_2^+ ions embedded in He_N. In Fig. 2(d), one can observe that the modulation amplitude of the first and second peak in the time-dependent yield distribution of HeD^+ were significantly decreased as compared to that of D^+ in Fig. 2(b), and the third peak was nearly smeared out. A comparable oscillatory tendency was observed for He_2D^+ as well. To have a quantitative analysis for the vibrational decaying feature, the experimental data points were fitted with the function $S(t) = S_0 + S_1 e^{-(t/t1)} + S_2 e^{-(t/t2)} \sin[2\pi(t - t_0)/T]$ [11,20]. The time constant t_1 represents the depletion of D_2^+ ions via dissociation to the continuum, and the t_2 accounts for the decay time constant of exponentially damped oscillations. In the fittings, by assuming a constant decay time t_1 (~29 fs) of D_2^+ dissociation for all conditions, the values of t_2 are obtained to be $\sim 25 \pm 8$ and 37 ± 6 fs for HeD^+ and D^+, respectively. This indicates a faster degeneration and stronger damping of the vibrational motion of the D_2^+ inside a droplet compared to that of the D_2^+ in the gas phase. For a gas-phase D_2^+, its vibrational motion is merely degenerated by the wave packet dispersion. However, for a D_2^+ ion immersed in the interior of He_N, additional strong perturbations to the vibrational dynamics raise up from the interaction between the dopant ion and the He environment.

Moreover, as shown in Fig. 2(e), the oscillation structures reflecting the quantum revival of the vibrational wave packet are absent for both yield signals of HeD^+ and He_2D^+ for time delay around 600 fs. Note that such structureless yield distributions of HeD^+ and He_2D^+ without periodic modulation have already occurred after ~140 fs. The corresponding frequency-domain representation of the NWP motion is plotted in the insert of Fig. 2(e). For the isolated gas-phase D_2^+, a dominant vibrational frequency of the D^+ signal is peaked at ~38.5 THz. However, for the in-droplet D_2^+, the lack of characteristic and dominant frequencies in the Fourier power spectrum implies a decoherence of the vibrational motion by the strong ion-He interaction.

In the previous studies, the investigated targets tend to be the neutral molecules sitting on the droplet surface or immersing in the He_N interior [17–19]. Since the interaction between the neutral molecule and droplet environment is considerably weak, their vibrational dynamics is weakly perturbed, leading to the observation of long-lived nuclear coherences [17]. However, for the here-studied in-droplet cation, the strong coupling of the excited ion to the surrounding He atoms will induce fast damping of the coherent vibrational motion, leading to the faster and irreversible decoherence of the NWP. The process of such

collisional dissipation dynamics of vibrational NWP of in-droplet ions is typically on a femtosecond timescale. In our study, by using the ultrafast vibrational motion of D_2^+ as a sensitive probe, such an ultrafast collisional dissipation process within ~140 fs is successfully visualized in real time.

To validate our assignment of the observed ultrafast vibrational decoherence of the in-droplet D_2^+ to the ion-He collisional interactions, we developed a semiclassical model to simulate the behavior of NWP decoherence inside a He_N. In the simulation model, the D_2^+-He_N system is simplified by considering 15 He atoms surrounding a D_2^+ ion. The open system model is given by the Liouville von-Neuman equation [50]

$$\frac{\partial \boldsymbol{\rho}}{\partial t} = i\hbar[\boldsymbol{H}, \boldsymbol{\rho}] - \frac{\boldsymbol{\rho} - \boldsymbol{\rho}^d}{\tau_0}. \quad (1)$$

The $\boldsymbol{\rho}$ is the density matrix of D_2^+. At the beginning, the initial density matrix is formed as $\boldsymbol{\rho}_{t=0} = |\nu_0\rangle\langle\nu_0|$, where v_0 is the vibrational ground state of neutral D_2. The $\boldsymbol{H}$ is the Hamiltonian containing both the diagonal and non-diagonal terms, which corresponds to the vibrational eigenstates of D_2^+, and the dipole-transition introduced by the probe pulse, respectively. The term of $[(\boldsymbol{\rho} - \boldsymbol{\rho}^d)/\tau_0]$ in the equation indicates the decoherence of NWP causing by the collisional effect of He_N on the D_2^+ vibrational motion, where the $\boldsymbol{\rho}^d$ is the diagonal term of $\boldsymbol{\rho}$, representing the vibrational eigenstates of D_2^+, and τ_0 is the decoherence time. The value of τ_0 is crucial in determining the vibrational decoherence dynamics of D_2^+ NWP in He_N.

Based on this simplified model, we performed the molecular dynamical simulations (see Supplemental Material [33] for more details). The critical value of $Dis_{He-D_2^+}$ representing the distance of the nearest He toward the D_2^+ was inspected. Each time the $Dis_{He-D_2^+}$ reaching a valley value represents the D_2^+ ion getting collided by a He atom. We iterated the molecular simulations for hundreds of times, and collected the time interval $T_{interval}$ between each He-D_2^+ collision. As displayed in Fig. 3(a), three typical routes with different initial conditions are presented, which results in different delay-dependent $Dis_{He-D_2^+}$ distributions. Figure 3(b) shows the extracted distribution of the $T_{interval}$ values. The most probable value of $T_{interval}$ ~ 59 fs can be regarded as the decoherence time τ_0, which is identified to be reliant on the mass of the molecular ions [33]. We note that this decoherence rate is comparable to the collision rate obtained from the Langevin model [33,41], which indicates the crucial role of ion-induced dipole interaction for the He-D_2^+ collision [42]. With τ_0 = 59 fs in Eq. (1), as shown in Fig. 3(c), the simulated time-dependent yield distribution of D^+, originating from the dissociation of D_2^+ ion suffering surrounding collisional interactions, exhibits a prominent vibrational structure with

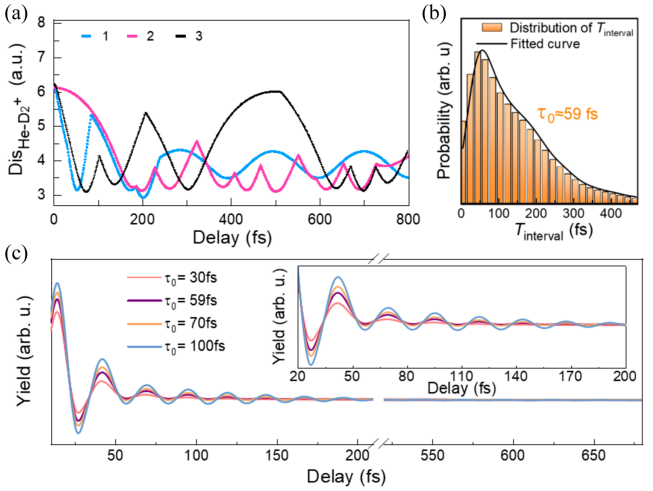

FIG. 3. (a) Simulated time-delay-dependent distance between the nearest He atom and D_2^+ ($Dis_{He-D_2^+}$). Three typical routes, labeled with 1, 2, 3 in different colors, represent different initial conditions. (b) Extracted distributions of time interval ($T_{interval}$) between each He-D_2^+ collision in the simulations. The orange histogram is the collected $T_{interval}$ distribution for the simulated collisional events. The black-solid curve shows the numerical fit to the simulation results based on kernel density estimation method. (c) Simulated yield distributions of He-perturbated D^+ as a function of time delay with different τ_0 values. The inset shows the enlarged distributions for delay between 20 and 200 fs.

fast decoherence within ~140 fs (purple solid line) and a flat distribution at larger time delay after 500 fs. The simulation results qualitatively agree with the experimental observations of the vibrational motion of the in-droplet D_2^+. Furthermore, to reveal the crucial role of τ_0 value in the collision-induced vibrational decoherence, we extracted the results for τ_0 = 30, 70 and 100 fs, respectively. As shown in Fig. 3(c), the smaller the τ_0 value is, the faster the D^+ yield distribution decays. This indicates that the more times the He-D_2^+ collision occurs, the stronger the perturbation is given by the He environment to the vibrational dynamics.

In general, the vibrational coherence loss of in-droplet dopants can be caused by both the elastic dephasing of the vibrational modes and the inelastic dephasing via droplet-induced relaxation of vibrational excitation. In the latter case, the dopant molecule strongly collides with the droplet, resulting in energy transfer from the molecule to the droplet environment and destruction of the coherent vibrational phase relations. Our observation is strikingly different from the previously observed long-lived vibrational coherences of in-droplet neutral indium dimers, where the elastic dephasing is mostly present [17]. The difference is rationalized by the different degrees of coupling of the molecular cations and neutral molecules to the He_N environment. In our recent studies, an enhanced dissociation of H_2^+ in He_N was observed, showing the participation of the surrounding He atom in the generation of HeH^+ ion [51]. The well depth of interaction potential of

He-H_2^+ ($\sim$2717 cm^{-1}) is much larger than that of He-H_2 ($\sim$10.3 cm^{-1}) [52,53]. The strong decoherence of NWP is partly due to the consumption of vibrationally excited D_2^+ populating on high lying states through the chemical reaction of $He + D_2^+ \rightarrow HeD^+ + D$.

To conclude, by real-time visualizing the vibrational NWP motion of the D_2^+ ion from the dissociative ionization of a D_2 molecule inside a He_N, we have demonstrated the observation of the extremely fast collisional dissipation dynamics, at timescales on the order of 100 fs. Our results show that, differing from the behaviors of the in-droplet neutral molecules, the charged ions in the He_N interior strongly couple to the He solvent via ion-He collisional interactions. The collision-induced dissipation of molecular dynamics is essential in diverse natural phenomena and technological applications, such as interstellar hydrogenation process [54], photosynthetic light harvesting [55,56], and quantum heat engines [57]. In particular, the observation of how the intermolecular collisions influence the excited molecular dynamics in a cold environment of He_N will pave the way for understanding the molecular reactions at extreme conditions, for instance, the collisional chemistry in the interstellar medium and planetary atmospheres.

This work was supported by the National Natural Science Fund (Grants No. 12227807, No. 12241407, No. 12304377, No. 12174109, No. 12074232, No. 12125406); the Science and Technology Commission of Shanghai Municipality (Grant No. 23JC1402000); Shanghai Pujiang Program (Grant No. 23PJ1402600); Jiangsu high-level talent plan (Grant No. JSSCBS20210218). J. Q. acknowledges the support from China Postdoctoral Innovation Talent Support Program (No. BX202320230331). L. Z. acknowledges the support from the Fundamental Research Funds for the Central Universities (No. YBNLTS2023-009) of East China Normal University in 2023. Y. P. acknowledges the National Science Key Lab Fund (Grant No. 6142A05200303). The authors acknowledge Mingchang Chen, Chin-Hsuan Lu, and Chia-Chen Hsu for helpful discussions on few-cycle laser pulses generation.

J. Q. and L. Z. contributed equally to this work.

*wbzhang@lps.ecnu.edu.cn
†jwu@phy.ecnu.edu.cn

[1] T. Vieillard, F. Chaussard, D. Sugny, B. Lavorel, and O. Faucher, Field-free molecular alignment of CO_2 mixtures in presence of collisional relaxation, J. Raman Spectrosc. **39**, 694 (2008).
[2] N. Owschimikow, F. Königsmann, J. Maurer, P. Giese, A. Ott, B. Schmidt, and N. Schwentner, Cross sections for rotational decoherence of perturbed nitrogen measured via decay of laser-induced alignment, J. Chem. Phys. **133**, 044311 (2010).
[3] P. Kukura, D. McCamant, S. Yoon, D. Wandschneider, and R. Mathies, Chemistry: Structural observation of the primary isomerization in vision with femtosecond-stimulated Raman, Science **310**, 1006 (2005).
[4] T. Joutsuka, W. H. Thompson, and D. Laage, Vibrational quantum decoherence in liquid water, J. Phys. Chem. Lett. **7**, 616 (2016).
[5] W. Miller, Perspective: Quantum or classical coherence?, J. Chem. Phys. **136**, 210901 (2012).
[6] J. Stenger, D. Madsen, P. Hamm, E. T. J. Nibbering, and T. Elsaesser, Ultrafast vibrational dephasing of liquid water, Phys. Rev. Lett. **87**, 027401 (2001).
[7] O. Cheshnovsky and A. Amirav, Lifetimes of electronically excited NO_2 in a collision-free differentially pumped supersonic molecular beam, Chem. Phys. Lett. **109**, 368 (1984).
[8] O. Sneh and O. Cheshnovsky, Triplet state interrogation in supersonic beams by surface electron ejection, Isr. J. Chem. **30**, 13 (1990).
[9] J. Ma, H. Zhang, B. Lavorel, F. Billard, E. Hertz, J. Wu, C. Boulet, J.-M. Hartmann, and O. Faucher, Observing collisions beyond the secular approximation limit, Nat. Commun. **10**, 5780 (2019).
[10] C. Meier and J. A. Beswick, Femtosecond pump-probe spectroscopy of I_2 in a dense rare gas environment: A mixed quantum/classical study of vibrational decoherence, J. Chem. Phys. **121**, 4550 (2004).
[11] Q. Liu, C. Wan, and A. Zewail, Solvation ultrafast dynamics of reactions. 13. Theoretical and experimental studies of wave packet reaction coherence and its density dependence, J. Phys. Chem. **100**, 18666 (1996).
[12] T. Joutsuka, W. Thompson, and D. Laage, Vibrational quantum decoherence in liquid water, J. Phys. Chem. Lett. **7**, 616 (2016).
[13] V. Balevičius Jr, T. Wei, D. Di Tommaso, D. Abramavicius, J. Hauer, T. Polívka, and C. Duffy, The full dynamics of energy relaxation in large organic molecules: From photo-excitation to solvent heating, Chem. Sci. **10**, 4792 (2019).
[14] A. Laubereau, D. von der Linde, and W. Kaiser, Direct measurement of the vibrational lifetimes of molecules in liquids, Phys. Rev. Lett. **28**, 1162 (1972).
[15] J. Qiang, L. Zhou, P. Lu, K. Lin, Y. Ma *et al.*, Femtosecond rotational dynamics of D_2 molecules in superfluid helium nanodroplets, Phys. Rev. Lett. **128**, 243201 (2022).
[16] D. Pentlehner, J. Nielsen, A. Slenczka, K. Mølmer, and H. Stapelfeldt, Impulsive laser induced alignment of molecules dissolved in helium nanodroplets, Phys. Rev. Lett. **110**, 093002 (2013).
[17] B. Thaler, M. Kappe, P. Heim, and M. Koch, Long-lived nuclear coherences inside helium nanodroplets, Phys. Rev. Lett. **124**, 115301 (2020).
[18] P. Claas, G. Droppelmann, C. Schulz, M. Mudrich, and F. Stienkemeier, Wave packet dynamics of K_2 attached to helium nanodroplets, J. Phys. B **39**, S1151 (2006).
[19] P. Claas, G. Droppelmann, C. Schulz, M. Mudrich, and F. Stienkemeier, Wave packet dynamics in triplet states of Na_2 attached to helium nanodroplets, J. Phys. Chem. A **111**, 7537 (2007).
[20] H. Schmidt, J. von Vangerow, F. Stienkemeier, A. Bogomolov, A. Baklanov, D. Reich, W. Skomorowski,

C. Koch, and M. Mudrich, Predissociation dynamics of lithium iodide, J. Chem. Phys. **142**, 044303 (2015).
[21] M. Y. Choi, G. E. Douberly, T. M. Falconer, W. K. Lewis, C. M. Lindsay, J. M. Merritt, P. L. Stiles, and R. E. Miller, Infrared spectroscopy of helium nanodroplets: Novel methods for physics and chemistry, Int. Rev. Phys. Chem. **25**, 15 (2006).
[22] A. S. Chatterley, L. Christiansen, C. A. Schouder, A. V. Jorgensen, B. Shepperson, I. N. Cherepanov, G. Bighin, R. E. Zillich, M. Lemeshko, and H. Stapelfeldt, Rotational coherence spectroscopy of molecules in helium nanodroplets: Reconciling the time and the frequency domains, Phys. Rev. Lett. **125**, 013001 (2020).
[23] R. M. P. Tanyag, B. Langbehn, T. Möller, and D. Rupp, in *Molecules in Superfluid Helium Nanodroplets: Spectroscopy, Structure, and Dynamics*, edited by A. Slenczka and J. P. Toennies (Springer International Publishing, Cham, 2022), p. 281.
[24] D. Bonhommeau, M. Lewerenz, and N. Halberstadt, Fragmentation of ionized doped helium nanodroplets: Theoretical evidence for a dopant ejection mechanism, J. Chem. Phys. **128**, 054302 (2008).
[25] M. Guhr, M. Bargheer, M. Fushitani, T. Kiljunen, and N. Schwentner, Ultrafast dynamics of halogens in rare gas solids, Phys. Chem. Chem. Phys. **9**, 779 (2007).
[26] R. Monni, G. Auböck, D. Kinschel, K. M. Aziz-Lange, H. B. Gray, A. Vlček, and M. Chergui, Conservation of vibrational coherence in ultrafast electronic relaxation: The case of diplatinum complexes in solution, Chem. Phys. Lett. **683**, 112 (2017).
[27] G. Douberly, K. Nauta, and R. Miller, The infrared spectrum of acetylene–HF in helium nanodroplets, Chem. Phys. Lett. **377**, 384 (2003).
[28] S. Kollotzek, J. Campos-Martínez, M. Bartolomei *et al.*, Helium nanodroplets as an efficient tool to investigate hydrogen attachment to alkali cations, Phys. Chem. Chem. Phys. **25**, 462 (2023).
[29] S. Smolarek, N. B. Brauer, W. J. Buma, and M. Drabbels, IR spectroscopy of molecular ions by nonthermal ion ejection from helium nanodroplets, J. Am. Chem. Soc. **132**, 14086 (2010).
[30] X. Zhang, N. B. Brauer, G. Berden, A. M. Rijs, and M. Drabbels, Mid-infrared spectroscopy of molecular ions in helium nanodroplets, J. Chem. Phys. **136**, 044305 (2012).
[31] J. Ullrich, R. Moshammer, A. Dorn, R. Dörner, L. Schmidt, and H. Schmidt-Böcking, Recoil-ion and electron momentum spectroscopy: Reaction-microscopes, Rep. Prog. Phys. **66**, 1463 (2003).
[32] P. Toennies and A. Vilesov, Superfluid helium droplets: A uniquely cold nanomatrix for molecules and molecular complexes, *Angew. Chem. (International ed. in English)* 43, 2622 (2004).
[33] See Supplemental Material at http://link.aps.org/supplemental/10.1103/PhysRevLett.132.103201 for details on experimental and simulational methods, and analysis, which includes Refs. [34–43].
[34] K. E. Riley and P. Hobza, Noncovalent interactions in biochemistry, WIREs Comput. Mol. Sci. **1**, 3 (2011).
[35] H. J. Werner, P. J. Knowles, F. R. Manby *et al.*, The Molpro quantum chemistry package, J. Chem. Phys. **152**, 144107 (2020).
[36] H. J. Werner and P. J. Knowles, An efficient internally contracted multiconfiguration–reference configuration interaction method, J. Chem. Phys. **89**, 5803 (1988).
[37] P. J. Knowles and H.-J. Werner, An efficient method for the evaluation of coupling coefficients in configuration interaction calculations, Chem. Phys. Lett. **145**, 514 (1988).
[38] K. Shamasundar, G. Knizia, and H.-J. Werner, A new internally contracted multi-reference configuration interaction (MRCI) method, J. Chem. Phys. **135**, 054101 (2011).
[39] R. J. Donnelly and C. F. Barenghi, The observed properties of liquid helium at the saturated vapor pressure, J. Phys. Chem. Ref. Data **27**, 1217 (1998).
[40] T. Ergler, A. Rudenko, B. Feuerstein, K. Zrost, C. D. Schröter, R. Moshammer, and J. Ullrich, Spatiotemporal imaging of ultrafast molecular motion: Collapse and revival of the D_2^+ nuclear wave packet, Phys. Rev. Lett. **97**, 193001 (2006).
[41] J. Glosík, Measurement of the reaction rate coefficients of reactions of H_2^+ with Ne, Ar, Kr, Xe, H_2, D_2, N_2 and CH_4 at thermal energy, Int. J. Mass Spectrom. Ion Process. **139**, 15 (1994).
[42] B. R. Eichelberger, T. P. Snow, and V. M. Bierbaum, Collision rate constants for polarizable ions, J. Am. Soc. Mass Spectrom. **14**, 501 (2003).
[43] J. Harms, J. P. Toennies, and F. Dalfovo, Density of superfluid helium droplets, Phys. Rev. B **58**, 3341 (1998).
[44] C.-H. Lu, Y.-J. Tsou, H.-Y. Chen, B.-H. Chen, Y.-C. Cheng, S.-D. Yang, M.-C. Chen, C.-C. Hsu, and A. Kung, Generation of intense supercontinuum in condensed media, Optica **1**, 400 (2014).
[45] P. Bucksbaum, A. Zavriyev, H. Muller, and D. Schumacher, Softening of the H_2^+ molecular bond in intense laser fields, Phys. Rev. Lett. **64**, 1883 (1990).
[46] T. Zuo and A. Bandrauk, Charge-resonance-enhanced ionization of diatomic molecular ions by intense lasers, Phys. Rev. A **52**, R2511 (1995).
[47] A. S. Alnaser, B. Ulrich, X. M. Tong *et al.*, Simultaneous real-time tracking of wave packets evolving on two different potential curves in H_2^+ and D_2^+, Phys. Rev. A **72**, 030702(R) (2005).
[48] R. W. Robinett, Quantum wave packet revivals, Phys. Rep. **392**, 1 (2004).
[49] I. A. Bocharova, H. Mashiko, M. Magrakvelidze, D. Ray, P. Ranitovic, C. L. Cocke, and I. V. Litvinyuk, Direct Coulomb-explosion imaging of coherent nuclear dynamics induced by few-cycle laser pulses in light and heavy hydrogen, Phys. Rev. A **77**, 053407 (2008).
[50] C. Zhu, A. Jasper, and D. Truhlar, Non-Born-Oppenheimer Liouville-von Neumann dynamics. evolution of a subsystem controlled by linear and population-driven decay of mixing with decoherent and coherent switching, J. Chem. Theory Comput. **1**, 527 (2005).

[51] L. Zhou, X. Hu, Y. Peng, J. Qiang, P. Lu *et al.*, Enhancing strong-field dissociation of H_2^+ in helium nanodroplets, Phys. Rev. Lett. **130**, 033201 (2023).

[52] M. Meuwly and J. M. Hutson, The potential energy surface and near-dissociation states of He-H_2^+, J. Chem. Phys. **110**, 3418 (1999).

[53] F. M. Tao, An accurate *ab initio* potential energy surface of the $He - H_2$ interaction, J. Chem. Phys. **100**, 4947 (1994).

[54] K. A. Korchagina, F. Spiegelman, and J. Cuny, Molecular dynamics study of the collision-induced reaction of H with CO on small water clusters, J. Phys. Chem. A **121**, 9485 (2017).

[55] H. Lee, Y.-C. Cheng, and G. R. Fleming, Coherence dynamics in photosynthesis: Protein protection of excitonic coherence, Science **316**, 1462 (2007).

[56] G. S. Engel, T. R. Calhoun, E. L. Read, T.-K. Ahn, T. Mančal, Y.-C. Cheng, R. E. Blankenship, and G. R. Fleming, Evidence for wavelike energy transfer through quantum coherence in photosynthetic systems, Nature (London) **446**, 782 (2007).

[57] M. O. Scully, K. R. Chapin, K. E. Dorfman, M. B. Kim, and A. Svidzinsky, Quantum heat engine power can be increased by noise-induced coherence, Proc. Natl. Acad. Sci. U.S.A. **108**, 15097 (2011).